

Nonlocality in Homogeneous Superfluid Turbulence

O. M. Dix and R. J. Zieve

Department of Physics, University of California Davis, Davis, California 95616, USA

Simulating superfluid turbulence using the localized induction approximation in periodic boundaries produces open-orbit vortices, which make superfluid turbulence unsustainable. Calculating with the fully nonlocal Biot-Savart law prevents the open-orbit state from forming, but also increases computation time. We use a truncated Biot-Savart integral to investigate the effects of nonlocality on homogeneous turbulence. We find that including the nonlocal interaction up to the average intervortex spacing prevents this open-orbit state from forming, yielding an accurate model of homogeneous superfluid turbulence with less computation time.

Superfluid helium can be described by a two-fluid model as comprised of a normal fluid part with velocity v_n and a superfluid part with velocity v_s . At small velocities, the superfluid exhibits remarkable properties such as the ability to flow without dissipation. But above some critical velocity, turbulence sets in and new interactions must be considered. Schwarz¹ provided a major computational breakthrough in understanding superfluid turbulence as a tangle of vortex filaments, an idea first suggested by Feynman² and investigated by Vinen³. Each vortex filament is an effectively one-dimensional curve around which superfluid flows. Since the superfluid is incompressible, $\nabla \cdot \vec{v}_s = 0$, the flow field due to these vortices is determined by the Biot-Savart law. Kelvin's theorem indicates that vortices move at approximately the local superfluid velocity, meaning that the motion of each segment of the vortex is determined by the positions of all vortices in the tangle. An additional interaction term between the superfluid vortex and the normal fluid gives us the vortex equation of motion:

$$\begin{aligned} \dot{\vec{s}}(\xi, t) = & \vec{v}_s + \dot{\vec{s}}_{\text{Biot}} + \alpha \hat{s}' \times (\vec{v}_{ns} - \dot{\vec{s}}_{\text{Biot}}) \\ & - \alpha' \hat{s}' \times \left[\hat{s}' \times (\vec{v}_{ns} - \dot{\vec{s}}_{\text{Biot}}) \right], \quad (1) \\ \dot{\vec{s}}_{\text{Biot}} = & \frac{\kappa}{4\pi} \int \frac{(\vec{s}_o - \vec{s}) \times d\vec{\xi}_o}{|\vec{s}_o - \vec{s}|^3}. \end{aligned}$$

Here, $\vec{s}(\xi, t)$ is the position along the vortex, parametrized by the arclength, ξ . The circulation κ is a fundamental constant for the superfluid vortex and the integral runs over all vortices within the tangle. The vector \hat{s}' is the unit vector tangent to the vortex filament, along which $d\vec{\xi}_o$ also points. α and α' are temperature-dependent parameters characterizing the interaction between the normal fluid and the vortex core, and the quantity \vec{v}_{ns} is equal to $\vec{v}_n - \vec{v}_s$.

The Biot-Savart integral diverges as the source point \vec{s}_o approaches the field point \vec{s} , so the integral is split into a local part and nonlocal part^{4,5}. The local part extends from the radius of the filament core, a_0 , to some arclength, l_{\pm} , away from the point of interest. The remaining part of the vortex system is included in the non-

local part of the integral,

$$\begin{aligned} \dot{\vec{s}}_{\text{Biot}}(\xi, t) = & \frac{\kappa}{4\pi} \hat{s}' \times \vec{s}'' \ln \left(\frac{2(l_+ l_-)^{1/2}}{e^{1/4} a_0} \right), \\ & + \frac{\kappa}{4\pi} \int' \frac{(\vec{s}_o - \vec{s}) \times d\vec{\xi}_o}{|\vec{s}_o - \vec{s}|^3}. \end{aligned}$$

Since the local term dominates, the nonlocal part has often been ignored. This is called the localized induction approximation (LIA) or the local approximation. When this is done, there is no objective best cutoff for l_{\pm} in the local term so the average radius of curvature, \bar{R} , is used and the coefficient in front of the local term is referred to as β , sometimes with a constant c of order unity included:

$$\beta = \frac{\kappa}{4\pi} \ln \left(\frac{\bar{R}}{c a_0} \right).$$

Vortex behavior is strongly influenced by vortex reconnections: vortices can approach and touch at a point, exchange heads and tails, then withdraw. Schwarz⁵ investigated these events, arguing that the process could be modeled by an instantaneous swap once two vortex segments approach within some cutoff distance. When the LIA is employed, vortex reconnections are the only nonlocal interaction involved in the simulation.

I. MOTIVATION: OPEN-ORBIT VORTICES

The issue we address in this paper was brought to light following the comments made by Buttke⁶ and Schwarz⁷; Buttke argued that use of the LIA and reconnection ansatz did not permit sustainable homogeneous turbulence, while Schwarz maintained that the simulation geometry was the problem: using all periodic boundaries allows vortices to reconnect with themselves while straddling periodic walls, leading to “open-orbit” vortices. Periodic boundary conditions in three dimensions identify opposing faces of a cube, resulting in a 3-torus. An open-orbit vortex wraps around one of the holes of this 3-torus, making it topologically distinct from any vortex that does not cross the cell boundary in this way. Conversion between the two vortex types requires a reconnection. The open-orbit vortex state can persist enough to destroy the

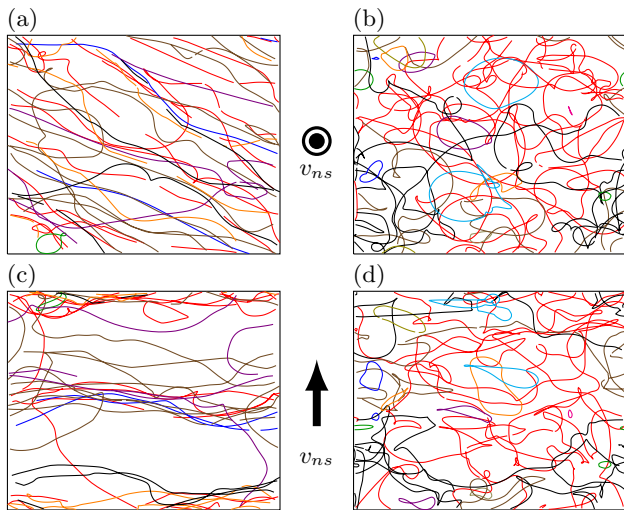


FIG. 1. Snapshots of vortex tangles from the present work with (a) side and (c) top views of the LIA calculation. (b) Side and (d) top views show similar snapshots using our calculations with the full Biot-Savart law. The figures use a periodic cube with side length $D = 0.005$ cm displayed at time $t = 0.115$ s.

usual homogeneous turbulence or prevent it from developing. Figure 1 shows the vortex tangle both in the open-orbit state and with typical homogeneous turbulent behavior. The structure of each part of this figure matches previous simulations⁸.

Different ways of addressing this phenomenon have arisen over the years. Schwarz⁹, using the LIA, showed that real-wall boundaries eliminate this problem. But periodic boundaries are much less computationally expensive and, thus, he inserted an occasional mixing step to sustain turbulence. Aarts¹⁰ focused on the time domain after the vortex line length equilibrated but before the system degenerated into the open-orbit state. The most physical solution was given by Adachi *et al.*⁸, who used the full Biot-Savart law, eliminating the need for special accommodations to fix or avoid the open-orbit state. By comparing to the LIA, Adachi *et al.*⁸ argued that the LIA is inadequate for simulating homogeneous superfluid turbulence.

In Section II we present data using the full Biot-Savart calculation to show that our code is in good agreement with previous simulations and experiment. Then, in Section III we present results using a range of nonlocal interaction distances, from the full Biot-Savart law to the LIA, and we address the argument made by Adachi *et al.*⁸, that the LIA is an inadequate approximation. While we agree that the LIA does not suffice, we find that only a small region of nonlocal interaction is needed to accurately model the system.

II. REPRODUCING HOMOGENEOUS TURBULENCE: THE FULL BIOT-SAVART LAW

We run simulations focusing on the temperature $T \approx 1.6$ K, which corresponds to $\alpha = 0.1$. We ignore α' since it is an order of magnitude smaller, and we use v_n as our driving velocity ($v_s = 0$) throughout this work to eliminate uniform vortex translation. Except as otherwise noted, we use a periodic cube with side length $D = 0.005$ cm. Our equation of motion is integrated using a Runge-Kutta-Fehlberg method (RKF54) with an adaptive time step. Our point spacing is also adaptive, depending on the local radius of curvature within the range $R/12 \leq l \leq R/5$. As the vortex grows and a particular point spacing exceeds the upper limit, we add a new point along a circular arc determined by the points that neighbor this overlarge spacing, as described by Schwarz⁵. Our reconnection ansatz is similar to that of Schwarz⁹.

We shall compare the LIA and full Biot-Savart calculations in multiple ways, including through visual inspection (as in Figure 1), using the line length density given by

$$L = \frac{1}{V} \int d\xi, \quad (2)$$

where V is the system volume, and with measures of the anisotropy given by⁹:

$$I_{\parallel} = \frac{1}{VL} \int [1 - (\hat{s}' \cdot \hat{r}_{\parallel})^2] d\xi, \quad (3)$$

$$I_{\perp} = \frac{1}{VL} \int [1 - (\hat{s}' \cdot \hat{r}_{\perp})^2] d\xi, \quad (4)$$

$$I_{\ell} \hat{r}_{\parallel} = \frac{1}{VL^{3/2}} \int \hat{s}' \times \hat{s}'' d\xi. \quad (5)$$

Here \hat{r}_{\parallel} and \hat{r}_{\perp} are unit vectors parallel and perpendicular to the \vec{v}_{ns} direction. As long as both directions perpendicular to the flow velocity are equivalent, the following relation is true regardless of tangle geometry: $I_{\parallel}/2 + I_{\perp} = 1$. Note also that if a vortex tangle is completely isotropic, $I_{\parallel} = I_{\perp} = 2/3$ and $I_{\ell} = 0$. If vortices lie entirely within planes normal to \vec{v}_{ns} , $I_{\parallel} = 1$, $I_{\perp} = 1/2$, and I_{ℓ} will depend on the structure of the vortices.

Figure 2 compares $L(t)$ and $I_{\parallel}(t)$ for calculations with the LIA and full Biot-Savart law. The data agree well with those of Adachi *et al.*⁸, with small differences arising from different system sizes and driving velocities. It is clear that the LIA data deviate significantly from those of the fully nonlocal calculation. The presence of nonlocal interactions reduces the vortex line length density. As Adachi *et al.*⁸ explain, the nonlocal interaction is strongest before and after a reconnection, when vortices are closest. The nonlocal term tends to repel two parallel vortex segments and attract antiparallel segments. Consequently, fewer parallel reconnections occur when the nonlocal interaction is included. Furthermore, reconnections between antiparallel segments produce sharp cusps

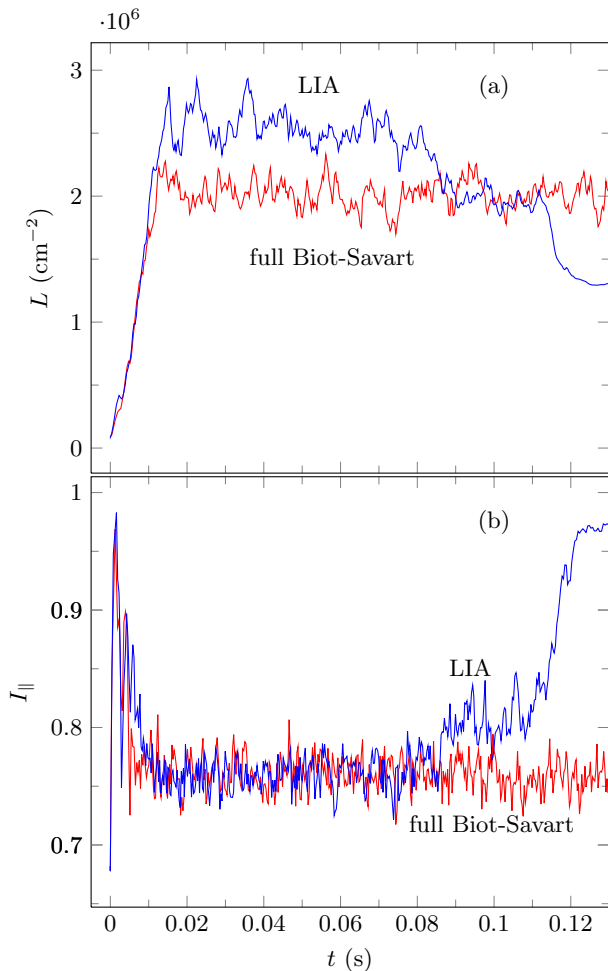


FIG. 2. Results from LIA and full Biot-Savart calculations for (a) $L(t)$ and (b) $I_{\parallel}(t)$, with $v_{ns} = 12$ cm/s.

that retreat away from the reconnection site quickly. By contrast, reconnections of parallel vortices result in more gently curved segments that do not retreat quickly. The net result of these effects is that the nonlocal interaction increases the average intervortex separation and correspondingly decreases the line length density.

Both $L(t)$ and $I_{\parallel}(t)$ indicate an apparently steady state-regime in the LIA calculations for $0.02 < t < 0.08$ s. Afterwards, the system settles into the open-orbit state, with vortices aligning perpendicular to the driving velocity as shown in Figure 1 (a) and 1 (c). Aarts¹⁰ observed a similar near-steady-state regime before open-orbit vortices appeared.

We demonstrate homogeneity of the full Biot-Savart calculation directly by finding the average line length density in different constituent volumes within the system (Equation 2). Figure 3 shows a sample evolution of $L(t)$. We use the eight \mathbb{R}^3 octants as the volumes to calculate each curve.

Even after steady-state turbulence has set in, we expect some variation in $L(t)$ among the octants, but the

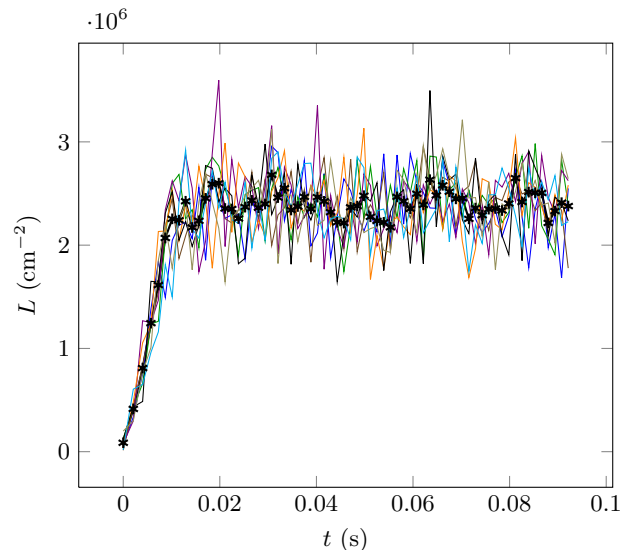


FIG. 3. Evolution of the vortex line length density, $L(t)$, within each octant of the periodic cube. The curve marked by black asterisks gives the line length per total system volume, D^3 . Each other curve gives $L(t)$ for one of the eight \mathbb{R}^3 octants. The applied velocity is $v_n = 12$ cm/s.

average equilibrated values should be the same. Figure 4 shows these average equilibrated L values for each octant, for a range of driving velocities. Time averages were done over the equilibrated time domain. We use the bracket notation $\langle X \rangle$ to denote the time average, as opposed to averages over the length of the vortex at a fixed time for which we use the notation \bar{X} . From Figure 4, it is clear that on this scale our system is homogeneous at every velocity.

Scaling arguments provide an additional test of homogeneous turbulence. Simple dimensional analysis shows that the line length density in homogeneous turbulence should depend on the driving velocity as⁹

$$\langle L \rangle = c_L^2 (v_{ns}/\beta)^2, \quad (6)$$

where c_L is temperature-dependent. As noted previously, β depends logarithmically on the average local radius of curvature, which decreases with increasing velocity. To keep c_L independent of velocity, we do not combine β with c_L . As shown in Figure 5, our simulations closely follow this scaling law. The best-fit value of c_L is 0.106.

Another scaling check of our simulations comes through the mutual friction force density due to interactions between the normal fluid and superfluid components. This force results in the interaction term of the vortex equation of motion (\vec{v}_{fric}),

$$\vec{F}_{sn} = -\frac{\rho_s \kappa}{V} \hat{s}' \times \vec{v}_{fric}, \quad (7)$$

where V is the system volume. When averaged along the entire vortex, only \vec{F}_{sn} parallel to the driving velocity is non-negligible. Schwarz⁹ also developed a scaling

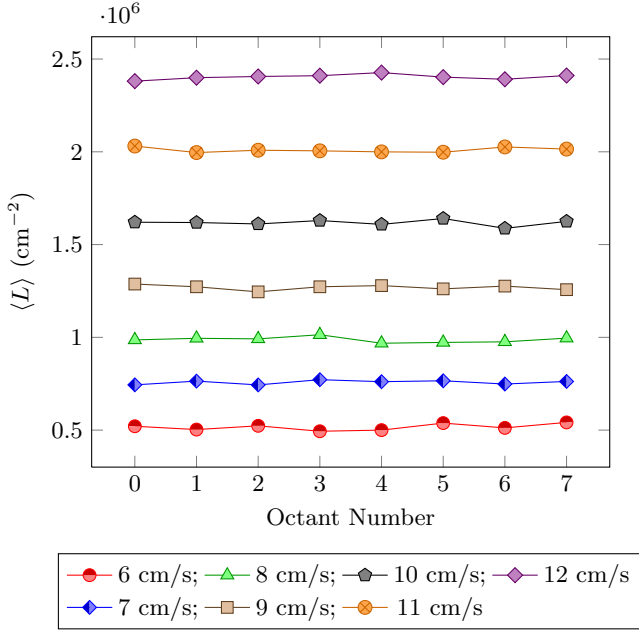


FIG. 4. Average equilibrated line length density, $\langle L \rangle$, within each octant of the periodic cube, at multiple velocities.

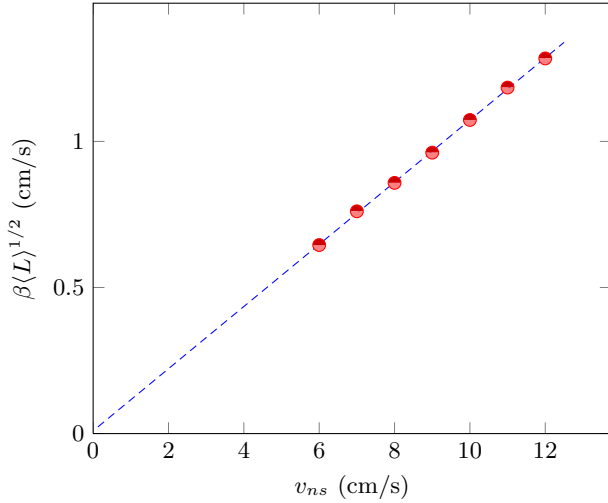


FIG. 5. Average equilibrated line length density, $\langle L \rangle$, for the total system volume, at multiple velocities. The linear fit to our data yields a slope of $c_L = 0.106$.

relation for the equilibrated force, $\langle \bar{F}_{sn} \rangle \propto v_{ns}^3 / \beta^2$. We construct a new quantity:

$$\bar{\Gamma} := \frac{\bar{F}_{sn}}{\rho_s \kappa \alpha v_{ns}}, \quad (8)$$

which we can fit in the form $\beta \langle \bar{\Gamma} \rangle^{1/2} = c_F v_{ns} + y_0$, as shown in Figure 6. The linear fit shows a slope of $c_F = 0.088$ with no y -intercept, as theory predicts.

Yet another quantity used to describe homogeneous superfluid turbulence is the average vortex velocity relative

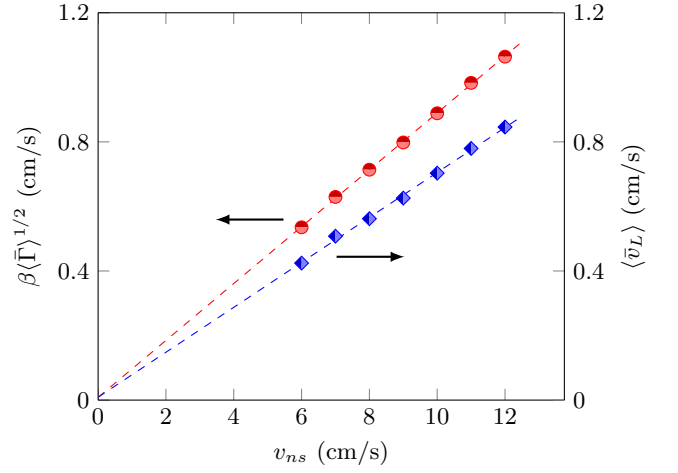


FIG. 6. Left axis (red circles): The quantity $\langle \bar{\Gamma} \rangle$ taken from the mutual friction force density, \bar{F}_{sn} along \hat{v}_{ns} . The linear fit of this data yields a slope of $c_F = 0.088$. Right axis (blue diamonds): The average vortex velocity, \bar{v}_L . The linear fit of this data yields a slope of $c_v = 0.070$.

to the applied superfluid velocity \vec{v}_s :

$$\bar{v}_L = \left[\frac{1}{VL} \int \mathbf{s} d\xi \right] - \vec{v}_s. \quad (9)$$

As for \bar{F}_{sn} , only the component of \bar{v}_L in the direction of the driving velocity is non-negligible. This time the quantity in question requires no scaling with β : $\bar{v}_L / v_{ns} = b(T)$, where $b(T)$ is a temperature-dependent parameter^{9,11}. Our data for \bar{v}_L are shown in Figure 6.

The anisotropy parameters from Equations 3 through 5 are also consistent with previous simulations: $\langle I_{\parallel} \rangle = 0.761$, $\langle I_{\perp} \rangle = 0.620$, $\langle I_{\ell} \rangle = 0.646$. These values show no significant trend over our range of v_{ns} . Schwarz⁹ points out that under the LIA, the average mutual friction force density \bar{F}_{sn} along \hat{v}_{ns} can be written as:

$$\bar{F}_{sn} = \rho_s \kappa \alpha (c_L^2 I_{\parallel} - c_L^3 I_{\ell}) v_{ns}^3 / \beta^2. \quad (10)$$

As we have defined it, then:

$$\bar{\Gamma} = (c_L^2 I_{\parallel} - c_L^3 I_{\ell}) \left(\frac{v_{ns}}{\beta} \right)^2.$$

We can see that the quantity, c_F , measured earlier from the mutual friction force density data is equal to $(c_L^2 I_{\parallel} - c_L^3 I_{\ell})^{1/2}$.

Equation 10 is only approximate when nonlocal contributions are included through the Biot-Savart law; hence we expect our calculations to produce slightly different values from those of Schwarz⁹ and Aarts¹⁰, who used the LIA. Additionally, Schwarz⁹ states that, when neglecting α' , the slope parameter we call c_v is equal to $c_L I_{\ell}$, again assuming the LIA. With these relations, we compare characteristics of homogeneous turbulence in our own simulations and in previous works, in Table I. We

use c_v or $c_L I_\ell$, depending on which can be derived from the data shown in earlier works. Similarly, we use c_F or $(c_L^2 I_\parallel - c_L^3 I_\ell)^{1/2}$. Schwarz⁹ does show that his theoretical calculations of I_\perp/I_\parallel , $(c_L^2 I_\parallel - c_L^3 I_\ell)^{1/2}$, and $c_L I_\ell$ match experiment.

Both Adachi *et al.*⁸ and Kondaurova *et al.*¹² report $\gamma = c_L/\langle\beta\rangle$ rather than c_L itself. Doing so requires one to insert an ad hoc y -intercept to maintain a decent linear fit. When we do this, we get a value of $\gamma = 137.3$ s/cm², where Adachi *et al.*⁸ report a value of $\gamma = 109.6$ s/cm². The experimental value is $\gamma = 93$ s/cm²^{11,13}. We can extract the value for $I_\perp/I_\parallel \approx 0.8$ from Adachi *et al.*⁸, which also matches our quantity from Table I of 0.815.

It should be noted that Kondaurova *et al.*¹² report $\gamma = 280$ s/cm², which is extremely high, as Adachi *et al.*⁸ mention. Kondaurova *et al.*¹² took the approach of applying the LIA, like Schwarz⁹, but modifying the reconnection ansatz to consider the velocity of vortex segments near reconnection sites. Reconnections could only occur if these vortex segments were expected to intersect based on their velocities. However, reconnections resulting in open orbits could still conceivably occur as a vortex grows through a boundary, back towards itself. Their large γ begs explanation and it is possible they simply did not run simulations for long enough to reach the open-orbit state. The use of the full Biot-Savart law by Adachi *et al.*⁸ is more plausible and gives better results.

Kondaurova *et al.*¹² also report values for the rate of vortex reconnections, an important process in carrying energy down to smaller length scales. Other simulations and analysis show the rate of vortex reconnections relates to the line length density as $\dot{n} = C\kappa\langle L\rangle^{5/2}$ where \dot{n} is the reconnection rate per unit volume and C is a dimensionless constant with a value of approximately 0.1-0.5¹⁴⁻¹⁶. Kondaurova *et al.*¹² report an exponent of 5/2 and an overlarge prefactor of $C = 2.47$. Figure 7 gives our data on the vortex reconnection rate for a series of trials. Analysis of this data yields an exponent of 2.47, and $C = 0.42$, within the normal range. Our full Biot-Savart calculation matches previous calculations of homogeneous superfluid turbulence through multiple comparisons.

III. NONLOCAL DISTANCE, d_{NL}

In this section, we investigate further the finding by Adachi *et al.*⁸ that the LIA approximation is inadequate for producing homogeneous turbulence. We saw in Figure 2 that despite the fact that L retains an approximate $\langle L\rangle \propto v^2$ relationship^{9,10}, and even in the time domain before the open-orbit vortex state dominates, L still deviates significantly between the LIA and full Biot-Savart calculations. The two methods do produce equally isotropic systems, however. For certain limited objectives, such as Schwarz's^{1,9} efforts to identify the attributes necessary for a given behavior, the LIA may be an acceptable approximation.

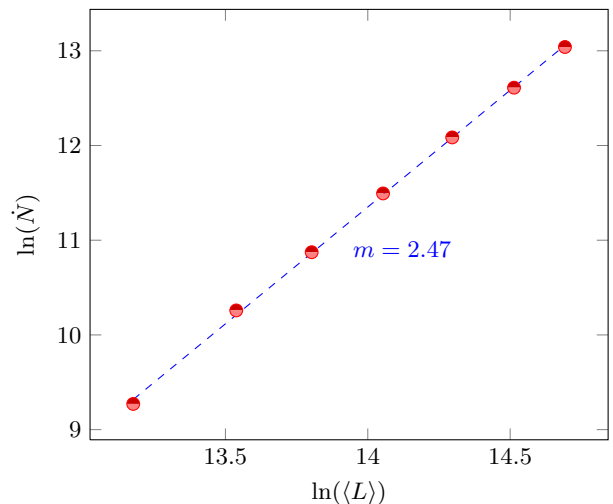


FIG. 7. A plot of $\ln(\dot{N})$ versus $\ln(\langle L\rangle)$, finding the exponent of $\dot{N} = dN/dt \propto \langle L\rangle^m$, $m = 2.47$.

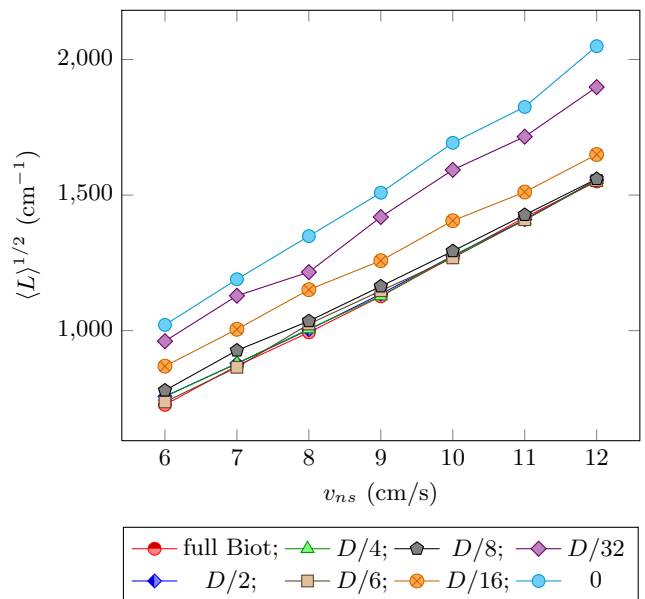


FIG. 8. Effects of nonlocal distance, d_{NL} , on the equilibrated line length density, $\langle L\rangle$. Each curve is a series of trials at the same d_{NL} , listed in the legend. The full Biot-Savart calculation has $d_{NL} = \sqrt{3}D/2$. Averages at each v_{ns} used the initial equilibrated dtg, similar to Aarts¹⁰.

Here we investigate whether some degree of the computation-saving power found in the LIA could be retained by truncating the maximum nonlocal interaction distance, which we denote with d_{NL} . For each point on the vortex, we only include contributions to the Biot-Savart integral, Equation 1, from other vortex segments that are within a distance d_{NL} . Our results for $\langle L\rangle^{1/2}(v_{ns})$ are displayed in Figure 8, for a range of d_{NL} values. The full Biot-Savart law is recovered at $d_{NL} = \sqrt{3}D/2$. As d_{NL} decreases from its maximum

Source (T=1.6 K)	c_L	I_{\perp}/I_{\parallel}	c_F	$(c_L^2 I_{\parallel} - c_L^3 I_{\ell})^{1/2}$	c_v	$c_L I_{\ell}$
Present Work	0.106	0.815	0.088	0.088	0.070	0.069
Aarts ¹⁰	0.11	-	0.095 [†]	-	0.045 [†]	-
Schwarz ⁹	0.137	0.775 [‡]	-	0.116 [†]	-	0.063 [†]

TABLE I. Comparison of quantities characterizing homogeneous turbulence. †: value calculated from other reported quantities; ‡: value estimated from published figure.

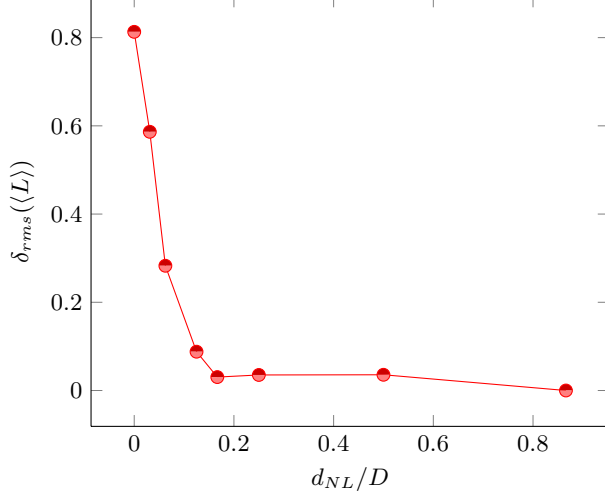


FIG. 9. RMS fractional deviation of $\langle L \rangle$ from the full Biot-Savart calculation for several nonlocal distances. The trials contributing to each point are from Figure 8, and use the initial equilibrated time domain for calculating the average of $L(t)$.

value, the data still remain remarkably similar to those using the full Biot-Savart law. Eventually the data begin to deviate. The onset of the divergence from the full Biot-Savart result is more apparent in Figure 9, which plots the root-mean-square (RMS) deviation of $\langle L \rangle$ from the full Biot-Savart value:

$$\delta_{rms}(\langle L \rangle) = \left\langle \left(\frac{\langle L \rangle - \langle L_{BS} \rangle}{\langle L_{BS} \rangle} \right)^2 \right\rangle_{v_{ns}}^{1/2}. \quad (11)$$

Here $\langle \dots \rangle_{v_{ns}}$ represents the average over trials with different v_{ns} values but the same d_{NL} . The quantity in Equation 11 acts as a measure of the error in our calculation due to the truncated nonlocal interaction. Figure 9 shows how this quantity varies with d_{NL} . This figure shows good agreement ($\lesssim 5\%$) between the full Biot-Savart calculation and those performed with a truncated nonlocal distance of at least $D/6$, but a clear departure arises by $D/8$.

These time averages all used the initial equilibrated time domain before the characteristic drop in $L(t)$, seen in Figure 2, i.e. before the degeneration into the open-orbit state occurs at the lower d_{NL} values. However, there is subjectivity in selecting the time domain over which to average $L(t)$ and this could potentially affect the critical d_{NL} . The drop in $L(t)$ when entering the open-

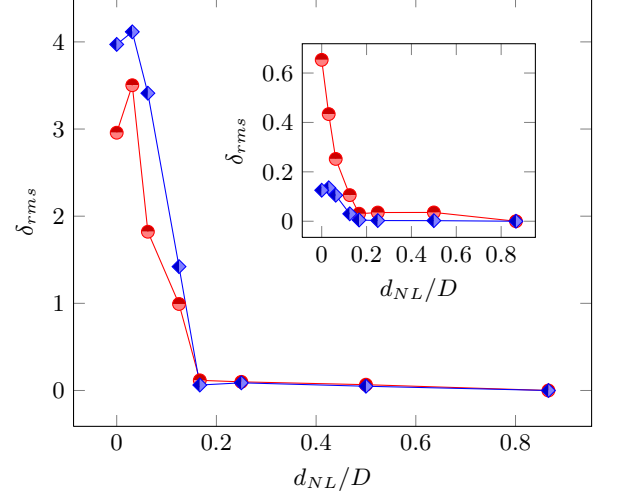


FIG. 10. RMS fractional deviation of the standard deviations $\sigma(L(t))$ (red circles) and $\sigma(I_{\parallel}(t))$ (blue diamonds) from the full Biot-Savart calculation plotted versus nonlocal distance. Inset: RMS fractional deviation of the averages $\langle L \rangle$ (red circles) and $\langle I_{\parallel} \rangle$ (blue diamonds) from the full Biot-Savart calculation plotted versus nonlocal distance. Averages use the entire equilibrated time domain. Compare $\langle L \rangle$ in the inset here to the data in Figure 9 to see the effects of what time domain is used for averaging.

orbit state also leads to an increase in the standard deviation of our $L(t)$ distribution. Thus, we can fit the entire equilibrated time domain and use the standard deviation of $L(t)$ as a parameter for measuring deviation from the full Biot-Savart calculation. From Figure 2, since I_{\parallel} only deviates from the full Biot-Savart value outside of the initial equilibrated range, we can now use this quantity and its standard deviation, as well. There is still a limited sample of data, since we cannot run trials forever, and we still have to pick out a time when the data start to equilibrate. Figure 10 shows the RMS fractional deviation of $\sigma(L(t))$, $\sigma(I_{\parallel}(t))$, $\langle L \rangle$, and $\langle I_{\parallel} \rangle$ (making the appropriate substitutions into Equation 11) for the trials from Figure 9 using the entire equilibrated time domain.

From the inset of Figure 10 we see that the critical d_{NL} value is $\lesssim D/6$, the same whether we use the entire equilibrated time domain in the averages of $L(t)$ and $I_{\parallel}(t)$ or simply the initial time domain, like in Figure 9. The main part of Figure 10 shows that the standard deviations of $L(t)$ and $I_{\parallel}(t)$ are very good parameters for measuring this critical d_{NL} , showing a pronounced increase in er-

ror for nonlocal distances below this same critical value. We can use a small fraction of the nonlocal interaction volume and still get a very good approximation of the Biot-Savart integral for homogeneous superfluid turbulence.

Reducing the interaction distance to such a degree can provide a considerable savings in computation time. With interactions omitted beyond $D/6$, the interaction volume for each vortex segment is about $1/50$ the full Biot-Savart calculation: each segment will have $1/50$ the number of other vortex segments contributing to its nonlocal velocity, when the system is homogeneous. Since other calculations must be performed for each point in the tangle, the end result is that simulations with the reduced interaction distance take $1/3$ to $1/10$ of the computation time.

We can see how error depends on driving velocity v_{ns} , for a fixed nonlocal distance d_{NL} . This breakdown of the data is shown in Figure 11 for $\langle L \rangle$ and $\sigma(L(t))$. For $\langle L \rangle$, deviations from the full nonlocal calculation are more pronounced at the lowest velocities for a fixed d_{NL} . For $\sigma(L(t))$ (and similarly for $\langle I_{\parallel} \rangle$ and $\sigma(I_{\parallel}(t))$, not shown), deviations are larger at higher velocities. The reason for this trend comes from what causes a calculation to differ from the full Biot-Savart law. At low velocities as d_{NL} is truncated from its maximum value, $\langle L \rangle$ is enhanced due to reduced repulsion and more reconnections between parallel vortices. Only at higher velocities do we see degeneration into the open-orbit state. The time at which this degeneration occurs decreases with increasing driving velocity so only at higher velocities does the degeneration occur within the time domain for which we run our simulations. When degeneration does occur, this drives the average $\langle L \rangle$ down closer to the value with the full Biot-Savart law.

Onset of the open-orbit state increases the standard deviations $\sigma(L(t))$ and $\sigma(I_{\parallel}(t))$, which explains why these two parameters deviate at higher velocities. Recall that $\langle I_{\parallel} \rangle$ for the LIA matches that of the full Biot-Savart calculations until onset of the open-orbit state (at about 0.08 s in Figure 2 (b)), explaining why deviation in this quantity is determined by onset of this state at higher velocities. From a practical perspective, regardless of the underlying cause of error, we want to choose an interaction distance such that every driving velocity we use produces turbulent behavior that matches the full Biot-Savart law. The RMS over all velocities at one d_{NL} picks out deviations at any v_{ns} .

We still need to be sure how this critical interaction distance varies with system size. It does not necessarily scale linearly. We simulated turbulence in two other system sizes, with other parameters held constant. $\langle L \rangle$ data for all three system sizes is shown in Figure 12. The good agreement in $\langle L \rangle$ for different system sizes is another mark of homogeneity. Since $\langle L \rangle$ is an intensive quantity, with a homogeneous system it must be independent of system size. Figure 13 shows the same quantities as Figure 10 but for $D = 0.0025$ cm and $D = 0.01$ cm.

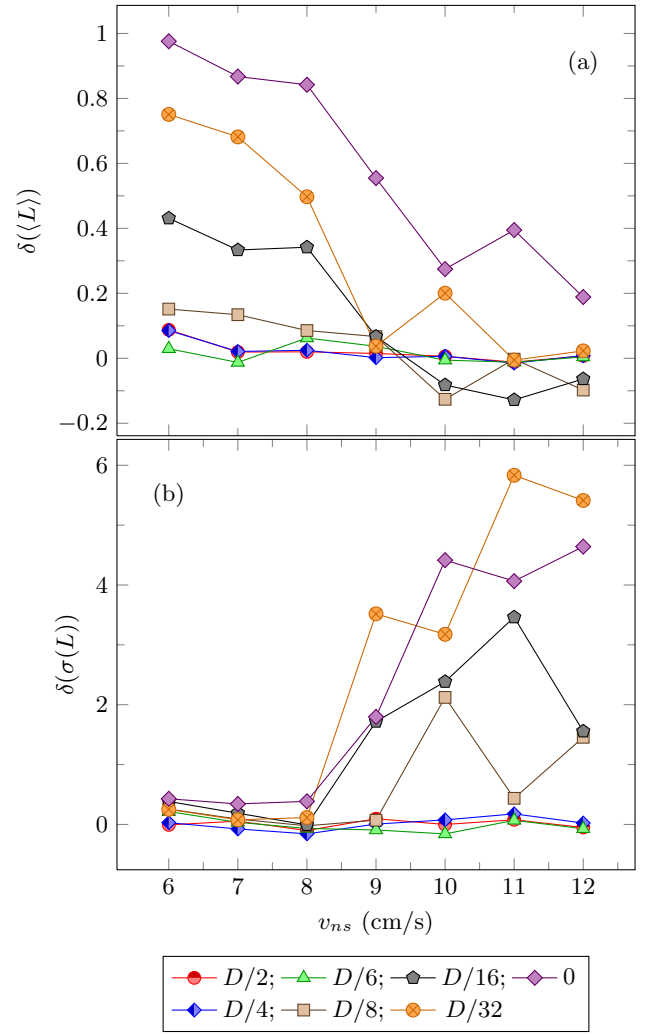


FIG. 11. Fractional deviation of (a) $\langle L \rangle$, and (b) $\sigma(L(t))$, from the full Biot-Savart calculation plotted versus driving velocity. Each curve is a different nonlocal distance, d_{NL} , indicated by the legend. Averages use the entire equilibrated time domain.

Simulations with system sizes $D = 0.0025$ cm and $D = 0.01$ cm have quantitatively similar behavior with varying d_{NL} as does $D = 0.005$ cm, in Figure 10. Both the averages and standard deviations of L and I_{\parallel} vary by only approximately 5% from the full nonlocal trials, until d_{NL} drops below $D/6$. From this, we can say that the interaction distance at which we regain the full Biot-Savart results should be approximately linear with system size, D . Any deviations from linearity should be small, given the factor of four change in D from 0.0025 cm to 0.01 cm with no detectable change in the critical d_{NL} .

The important question remains: why $D/6$? A simple argument can be made that the important physical length scale should be the average intervortex distance, which we can get from $\langle \ell \rangle = \langle L \rangle^{-1/2}$. The quantity $(\langle \ell \rangle - d_{NL})/D$ should serve as a useful indicator of whether we expect variation from the fully nonlocal cal-

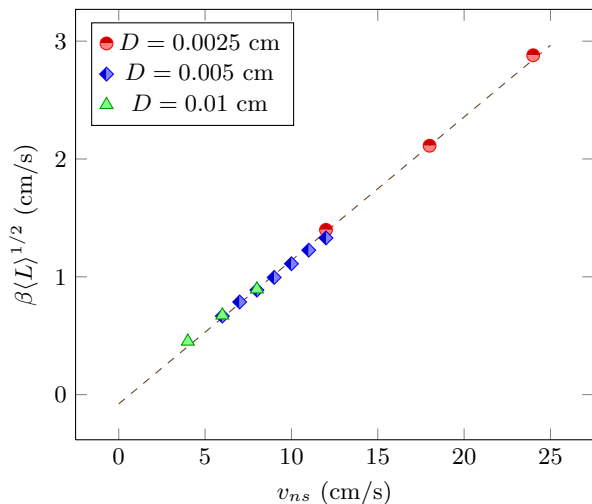


FIG. 12. $\beta \langle L \rangle^{1/2}$ data for all system sizes, $D = 0.0025, 0.005$, and 0.01 cm. Averages use the entire equilibrated time domain.

culation. The RMS fractional deviation of $\langle L \rangle$, $\sigma(L)$, $\langle I_{\parallel} \rangle$, and $\sigma(I_{\parallel})$ from the full Biot-Savart calculation is plotted versus this quantity in Figure 14, which shows that error in the simulation drastically increases when the nonlocal distance falls below the average intervortex spacing. As the nonlocal interaction distance is decreased to the average vortex separation distance, interactions between vortices cannot accurately simulate homogeneous superfluid turbulence.

Physically, this elucidates the importance of nonlocal interactions only up to the average intervortex spacing. Beyond this distance, the nonlocal contribution is apparently negligible. This makes sense, since the general form of the Biot-Savart law does show that nearest-neighbor interactions should dominate the nonlocal field. Our findings also makes sense for the open-orbit problem, in particular. The occasional open-orbit vortex would not necessarily doom a simulation with periodic boundaries if neighboring vortices are oriented in a way so a reconnection can free the vortex from this open-orbit state. This is evidenced by the occasional mixing step that Schwarz⁹ used to address the open-orbit problem. The state only persists indefinitely when neighboring vortices reconnect, each one with itself, to ultimately form an array of parallel and antiparallel vortices. Our findings support the notion that the degree of randomness between nearest-neighbor vortices is enough to prevent the simultaneous degeneration of vortices into the open-orbit state.

Adachi *et al.*⁸ showed the importance of the nonlocal interaction for homogeneous superfluid turbulence behavior, especially when simulating this system using periodic boundaries. By using a truncated Biot-Savart integral, we have found it is possible to regain some of the time saved with the localized induction approximation yet still accurately model the system behavior. Our findings argue that the nonlocal interaction is only important

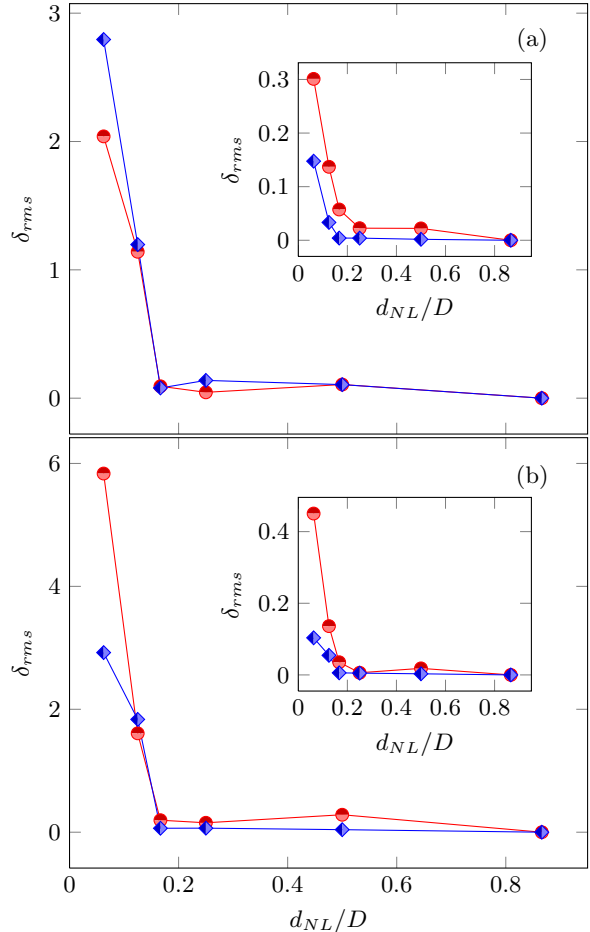


FIG. 13. For comparison with Figure 10: Figure (a) has system size $D = 0.0025$ cm, Figure (b) has $D = 0.01$ cm. RMS fractional deviation of the standard deviations $\sigma(L(t))$ (red circles) and $\sigma(I_{\parallel}(t))$ (blue diamonds) from the full Biot-Savart calculation plotted versus nonlocal distance. Insets: RMS fractional deviation of $\langle L \rangle$ (red circles), and $\langle I_{\parallel} \rangle$ (blue diamonds) from the full Biot-Savart calculation plotted versus nonlocal distance. Time averages use the entire equilibrated time domain.

up to distances of about the intervortex spacing.

¹ K. W. Schwarz, Physical Review Letters **49**, 283 (1982).

² R. P. Feynman, *Progress in Low Temperature Physics*, edited by C. Gorter, Vol. 1 (North Holland, 1955) p. 17.

³ W. F. Vinen, Proceedings of the Royal Society A **242**, 493

(1957).

⁴ R. J. Arms and F. R. Hama, The Physics of Fluids **8**, 553 (1965).

⁵ K. W. Schwarz, Physical Review B **31**, 5782 (1985).

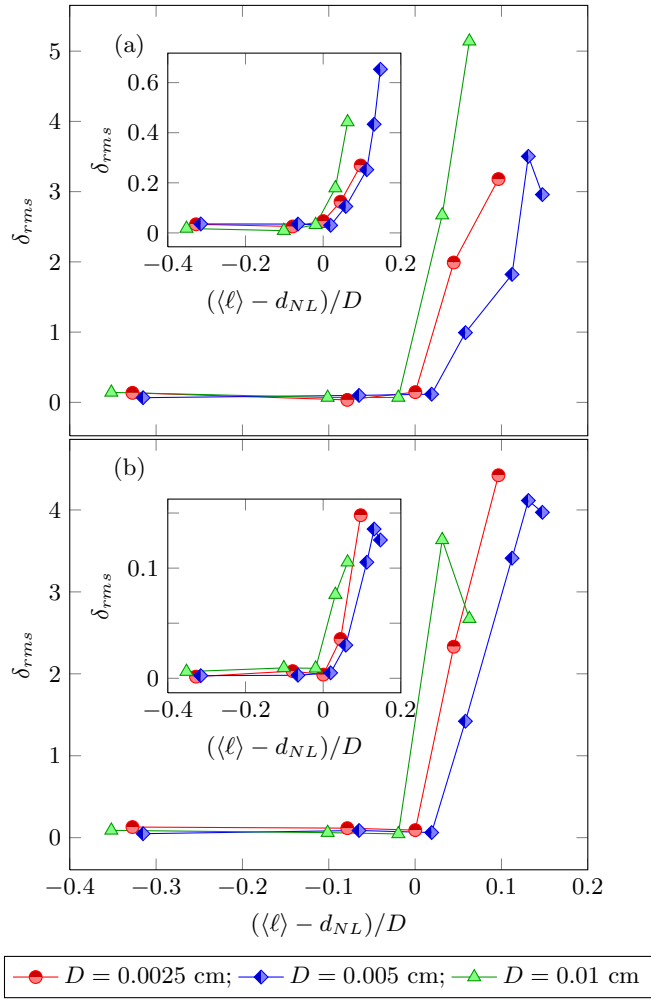


FIG. 14. RMS fractional deviation from the full Biot-Savart law of (a) the standard deviation $\sigma(L(t))$, (a) inset: the average $\langle L \rangle$, (b) $\sigma(I_{\parallel}(t))$, and (b) inset: $\langle I_{\parallel} \rangle$ plotted versus the difference between the average intervortex spacing and non-local distance. Each curve within a graph is for a different system size D , as indicated within the legend. Every point within a curve uses the average $\langle \ell \rangle$ for the range of v_{ns} trials for a single d_{NL} value.

- ⁶ T. F. Buttke, Physical Review Letters **59**, 2117 (1987).
- ⁷ K. W. Schwarz, Physical Review Letters **59**, 2118 (1987).
- ⁸ H. Adachi, S. Fujiyama, and M. Tsubota, Physical Review B **81**, 104511 (2010).
- ⁹ K. W. Schwarz, Physical Review B **38**, 2398 (1988).
- ¹⁰ R. Aarts, *A numerical study of quantized vortices in He II*, Ph.D. thesis, Eindhoven University of Technology (1993).
- ¹¹ J. Tough, *Progress In Low Temperature Physics*, edited by D. F. Brewer, Vol. VIII (North-Holland Publishing Company, 1982).
- ¹² L. P. Kondaurova, V. A. Andryuschenko, and S. K. Nemirovskii, Journal of Low Temperature Physics **150**, 415 (2008).
- ¹³ R. K. Childers and J. T. Tough, Physical Review B **13**, 1040 (1976).
- ¹⁴ M. Tsubota, T. Araki, and S. K. Nemirovskii, Physical Review B **62**, 11751 (2000).
- ¹⁵ C. Barenghi and D. Samuels, Journal of Low Temperature Physics **136**, 281 (2004).
- ¹⁶ S. K. Nemirovskii, Physical Review Letters **96**, 015301 (2006).